A histone methylation-MAPK signaling axis drives durable epithelial-mesenchymal transition in hypoxic pancreatic cancer

Brooke A. Brown[1], Paul J. Myers[1], Sara J. Adair[2], Jason R. Pitarresi[3], Shiv K. Sah-Teli[4], Logan A. Campbell[5], William S. Hart[1], Michelle C. Barbeau[6], Kelsey Leong[7], Nicholas Seyler[1], William Kane[2], Kyoung Eun Lee[8], Edward Stelow[9], Marieke Jones[10], M. Celeste Simon[11,12], Peppi Koivunen[4], Todd W. Bauer[2], Ben Z. Stanger[3], Matthew J. Lazzara[1,5]

[1] Department of Chemical Engineering, University of Virginia, Charlottesville, VA 22903, USA,
[2] Department of Surgery, University of Virginia, Charlottesville, VA 22903, USA
[3] Department of Medicine, University of Pennsylvania, Philadelphia, PA 19104, USA
[4] Faculty of Biochemistry and Molecular Medicine, Biocenter Oulu, University of Oulu, Oulu, FIN-90014, Finland
[5] Department of Biomedical Engineering, University of Virginia, Charlottesville, VA 22903, USA
[6] Biomedical Sciences, University of Virginia, Charlottesville, VA 22903, USA
[7] Engineering Science, University of Virginia, Charlottesville, VA 22903, USA
[8] Department of Pharmacology, University of Michigan, Ann Arbor, MI 48109, USA
[9] Department of Pathology, University of Virginia, Charlottesville, VA 22903, USA
[10] Claude Moore Health Sciences Library, University of Virginia, Charlottesville, VA 22903, USA
[11] Abramson Family Cancer Research Institute, University of Pennsylvania, Philadelphia, PA 19104, USA,
[12] Department of Cell and Developmental Biology, University of Pennsylvania, Philadelphia, PA 19104, USA

Running Title: Hypoxia Drives EMT in Pancreas Cancer

Keywords: extracellular signal-regulated kinases, JUN kinase, hypoxia-inducible factors, E-cadherin, vimentin, PP2A, PP2C

Abbreviations: Clinical Proteomic Tumor Analysis Consortium (CPTAC); epithelial-mesenchymal transition (EMT); gene set variation analysis (GSVA); Kyoto Encyclopedia of Genes and Genomes (KEGG); *Kras*$^{LSL-G12D}$, p53$^{LSL-R172H}$, Pdx1-Cre, Rosa26$^{LSL-YFP}$ (KPCY); mitogen-activated protein kinase (MAPK); pancreatic ductal adenocarcinoma (PDAC); patient-derived xenograft (PDX); The Cancer Genome Atlas (TCGA)

Conflicts of interest: The authors declare no conflicts of interest.

Corresponding Author:
Matthew J. Lazzara
385 McCormick Road
Charlottesville, VA 22903
Phone: 434-243-9767
E-mail: mlazzara@virginia.edu

ABSTRACT

The tumor microenvironment in pancreatic ductal adenocarcinoma (PDAC) plays a key role in tumor progression and response to therapy. The dense PDAC stroma causes hypovascularity, which leads to hypoxia. Here, we showed that hypoxia drives long-lasting epithelial-mesenchymal transition (EMT) in PDAC primarily through a positive-feedback histone methylation-MAPK signaling axis. Transformed cells preferentially underwent EMT in hypoxic tumor regions in multiple model systems. Hypoxia drove a cell-autonomous EMT in PDAC cells which, unlike EMT in response to growth factors, could last for weeks. Furthermore, hypoxia reduced histone demethylase KDM2A activity, suppressed PP2 family phosphatase expression, and activated MAPKs to post-translationally stabilize histone methyltransferase NSD2, leading to an H3K36me2-dependent EMT in which hypoxia-inducible factors played only a supporting role. Hypoxia-driven EMT could be antagonized *in vivo* by combinations of MAPK inhibitors. Collectively, these results suggest hypoxia promotes durable EMT in PDAC by inducing a histone methylation-MAPK axis that can be effectively targeted with multi-drug therapies, providing a potential strategy for overcoming chemoresistance.

STATEMENT OF SIGNIFICANCE

Integrated regulation of histone methylation and MAPK signaling by the low-oxygen environment of pancreatic cancer drives long-lasting EMT that promotes chemoresistance and shortens patient survival and that can be pharmacologically inhibited.

INTRODUCTION

The pancreatic ductal adenocarcinoma (PDAC) microenvironment exerts complex regulation of tumor progression and response to therapy. A well described feature of the PDAC stroma is its characteristic hypovascularity, which gives rise to low-oxygen subdomains (1,2). Hypoxic regions are found in most human PDAC, with oxygen tensions as low as 0.4% compared to 6.8% in adjacent normal tissue (1). Evidence of hypoxia is found at the pancreatic intraepithelial neoplasia (PanIN) stage, and sparse mature vasculature or pronounced hypoxia signatures portend shorter patient survival (2-4). Hypovascularity limits tumor access to systemic therapies and immune cells (2) and correlates with spontaneous metastasis (5). Hypoxia is also a purported driver of epithelial-mesenchymal transition (EMT) (6,7), which occurs as early as the late PanIN stage and is linked to chemoresistance and poor differentiation (8,9). All common PDAC classification systems identify an especially aggressive subtype enriched for mesenchymal characteristics (10-13).

Cytokines including transforming growth factor β (TGFβ), activin-A, and hepatocyte growth factor (HGF) are the best known EMT drivers (14,15). Beyond the ability of TGFβ to induce expression of EMT transcription factors, complete TGFβ-mediated EMT in PDAC cells also requires H3K36 dimethylation mediated by loss of histone lysine demethylase KDM2A and augmented expression of histone methyltransferase NSD2 (16). Hypoxia also promotes histone methylation (17), but the impact on EMT is unexplored. KDM5A and KDM6A are markedly inactivated by low oxygen (18,19), raising the possibility of an entirely intracellular mechanism for EMT in hypoxia.

Direct mechanistic evidence for hypoxia-driven EMT in PDAC is limited. Hypoxia-inducible factors (HIFs) may participate by driving *Twist* expression (6) or Wnt/β-catenin crosstalk (7), and *HIF1A* expression correlates with EMT transcriptomic signatures (20). The connection between hypoxia and specific EMT-promoting signaling pathways is largely unexplored. MAPKs are critical regulators of growth factor-driven EMT (14,21), but the potential

relevance of MAPKs in hypoxic PDAC cells and tumors for EMT has not been thoroughly investigated.

Here, we demonstrate that hypoxia promotes a *bona fide* EMT in PDAC via an integrated histone methylation and MAPK signaling mechanism. Human patient data show that the relationship between low oxygen and PDAC EMT is so typical that statistically significant relationships between EMT and hypoxia gene signatures exist. In mouse and cell culture models, hypoxia-mediated EMT occurs, can proceed in cell-autonomous fashion, and is more durable than growth factor-mediated EMT. The identification of MAPK signaling as indispensable for hypoxia-mediated EMT nominates specific targeted inhibitors for combination therapy approaches that could promote PDAC chemoresponse.

MATERIALS & METHODS

Data Analytics and Computational Modeling

Software and pre-processing of published publicly available data

R version 4.1.2 was used for analysis. See **Supp Table S1** for details on software packages used. See *Data Availability* for information on how data were obtained. For CPTAC proteomics, imputation was performed for proteins with non-missing values in ≥ 50% of samples using *DreamAI*. TCGA PAAD RNA-seq gene expression data were converted from $\log_2$(RSEM+1) normalized counts to transcripts per million (TPM) and then to $\log_2$(TPM+1). For TCGA PAAD phenotype and survival data, only PDAC tumors were retained (150 tumors), based on histological annotations.

Gene sets and signatures

Pan-cancer EMT (pcEMT) (22) or HIF target (23) signatures were used for most clustering. Gene sets from the Molecular Signatures Database and Kyoto Encyclopedia of

Genes and Genomes (KEGG) were accessed in R using *msigdbr* and *clusterProfiler*, respectively.

Clustering

Non-negative matrix factorization (NMF) of bulk tumor data from TCGA and CPTAC was performed with expression data for all available genes or proteins, respectively, based on the pcEMT signature using the *NMF* package. For CPTAC, data were used with imputation. Optimal NMF factorization rank *k* was selected as discussed in Supplementary Data. scRNA-seq data (24) was clustered through sequential 2D UMAP projection using pcEMT mesenchymal gene expression data (*umap* R package, nearest neighbors setting of 30, minimum distance of 0.01) followed by consensus clustering (*ConsensusClusterPlus* using Euclidean distance, Ward's linkage for subsampling and linkage method, and partitioning around medoids (PAM) algorithm).

Gene set enrichment and pathway overdispersion analysis

Gene set variation analysis (GSVA) was used to calculate enrichment scores using CPTAC PDAC global proteome and TCGA PAAD RNA-seq data (*GSVA* R package). For CPTAC data, global proteome data were used without imputation. For TCGA PAAD data, $\log_2$(TPM+1) expression values were used. Pathway and gene set overdispersion analysis (Pagoda2) was used to calculate gene set enrichment scores for ductal cell scRNA-seq data (24) using *Pagoda2*.

Overrepresentation analysis

Gene-equivalent protein phosphorylation data (all phosphosites, as provided by CPTAC) were filtered to retain kinases (358). Spearman rank correlation coefficients were calculated for kinase phosphorylation levels and Hallmark Hypoxia GSVA scores computed from CPTAC global proteomics. KEGG pathway overrepresentation analysis was then performed on

positively and significantly ($p < 0.05$) correlated phospho-kinases using *clusterProfiler*. Only the available kinases in CPTAC phosphoproteomics data were used for testing overrepresentation. *p* values were adjusted for multiple comparisons by controlling the false discovery rate. Spearman correlations and *p* values were calculated using *Hmisc*.

Statistical analyses and data visualization using R

ggstatsplot was used to perform Mann-Whitney U and Kruskal-Wallis tests, and the *survival* and *survminer* packages were used for log-rank test *p* values and survival curves, respectively. *ggplot2*, *tidyHeatmap*, *ComplexHeatmap* and *cowplot* were used for figures. UpSet plots were created using *ggupset*.

Additional computational methods information

Additional computational methods references are provided in Supplementary Data. Information on R packages is provided in **Supp Table S1**. The KEGG signaling pathways used for analyses are listed in **Supp Table S2**.

Experimental Methods

Patient-derived xenografts

PDAC tumor sample MAD12-395 was generated from a human pathology specimen coordinated through the UVA Biorepository and Tissue Research Facility (25). Tumors were passaged in mice, sewn orthotopically into 6-7-week-old female athymic nude mice (Envigo, Indianapolis, IN), and allowed to grow for 6 weeks until palpable. Dosing with inhibitors is described in Supplementary Data.

Autochthonous models and subcutaneous tumors using KPCY cell lines

For autochthonous studies, female and male *Kras*$^{LSL\text{-}G12D}$*, p53*$^{LSL\text{-}R172H}$*, Pdx1-Cre, Rosa26*$^{LSL\text{-}YFP}$ (KPCY) mice (8) were used. Mice were palpated and examined for morbidity twice per week. For subcutaneous tumors, female C57BL/6J (stock no. 000664) or NOD.SCID (stock no. 001303) mice were obtained from The Jackson Laboratory. C57BL/6J (7160c2) or mixed genetic background (PD7591) KPCY cell lines were previously described (9). 2×10^5 cells were injected subcutaneously and grew for 2-6 weeks, with 6 weeks used unless noted.

HPAF-II hypoxia fate-mapping orthotopic tumors

HPAF-II cells were engineered with a fate mapping system that enables an irreversible switch from DsRed to GFP expression in hypoxia (26) (Danielle Gilkes, Johns Hopkins). Cell engineering and clonal selection are described in Supplementary Data. To create tumors, 1×10^6 hypoxia fate-mapping HPAF-II cells were injected orthotopically in 8 week-old male athymic nude mice (Envigo, Indianapolis, IN). Mice were sacrificed 5 weeks later. Animal studies and procedures were approved by the University of Virginia Institutional Animal Care and Use Committee. Following sacrifice, tumor pieces were dissociated on ice followed by flow sorting, as described in Supplementary Data.

Detecting hypoxia in tumors

For all mouse tumor studies probing for hypoxia, pimonidazole was injected (IP, 60 mg/kg; Hypoxyprobe, catalog no. HP7-100) 90 min prior to tumor harvest.

Pathologic assessment of human tumors

Tumors were fixed in zinc-buffered formalin for 24 hr and paraffin-embedded. H&E staining was performed, and a board-certified pathologist (E.S.) assessed differentiation as “well”, “moderate”, or “poor”.

Cell culture

HPAF-II cells (Carl June, University of Pennsylvania) and PDX-derived cell lines (25) were maintained in RPMI. MiaPaca2 cells (Paolo Provenzano, University of Minnesota) were maintained in DMEM. Murine KPCY cells derived from *Kras*$^{LSL\text{-}G12D}$*, p53*$^{LSL\text{-}R172H}$*, Pdx1-Cre, Rosa26*$^{LSL\text{-}YFP}$ mice (2838c3, 6499c4, 6556c6, and 7160c2; all clonal) or *Kras*$^{LSL\text{-}G12D}$, *p53*$^{loxP/+}$, *Pdx1-Cre*, *Rosa26*$^{LSL\text{-}YFP}$ mice (PD798 and PD7591) were maintained in DMEM + GlutaMAX. Media were supplemented with 10% FBS, 1 mM L-glutamine, 100 units/mL penicillin, and 100 µg/mL streptomycin. Murine cell media was also supplemented with 8.66 µg/mL gentamicin. Mycoplasma testing of HPAF-II and PDX cell line stocks was done using the MycoAlert PLUS Detection Kit (Lonza) (July-October 2020). HPAF-II cells were authenticated by the Genetic Resources Core Facility at Johns Hopkins University by short tandem repeat profiling (February 2022). Cells were used within 15 passages of thawing frozen vials. Cells were maintained at 5% CO_2 and 37ºC in a Thermo Scientific Forma Steri-Cycle i160 incubator (21% O_2) or Tri-Gas Steri-Cycle i160 (1% or 7% O_2). For hypoxia experiments, cells were moved to 1% O_2 16 hr after plating, and medium was changed after 72 hr, or every 48 hr when growth factors or inhibitors were used. Cells were treated with inhibitors immediately prior to hypoxic culture.

Fluorescence microscopy (cell culture and tissues) and automated image analysis

Slides were imaged on a Zeiss Axiovert Observer.Z1 fluorescence microscope, using a 10, 20, or 40× objective and ZEN software. Comparisons used identical exposure times and image settings. For each replicate coverslip, four frames were taken randomly, and at least 1000 cells were quantified. For immunohistochemistry, ≥ 8 frames per tumor section were taken. CellProfiler v3.1.9 (Broad Institute) (27) was used to quantify signal intensity and localization. See Supplementary Data for additional details.

Statistical analyses

Graphpad Prism 9 for macOS was used for statistical analyses. Vimentin/E-cadherin linear least squares regression was performed without weighting with F test comparison to a line of zero slope. Cell scatter logistic least squares regressions were performed with F test comparison between 21% and 1% O_2. For two-way ANOVA, Tukey's multiple comparisons or Sidak's multiple comparisons tests were used when considering all conditions or only specific conditions, respectively. For single-cell protein measurements, a mixed-effects model was used where the number of biological replicates taken as the *n* value and individual cells were treated as repeated measurements within biological replicates.

Additional experimental methods information

Additional information on methods and reagents, including methodological references, are in the Supplementary Data. Primer sequences for quantitative real-time PCR are provided in **Supp Table S3**.

Ethics

All animal work conformed to standards of good research practice, and animals were maintained in compliance with NIH guidelines. For autochthonous and subcutaneous tumor models, experiments were approved by the University of Pennsylvania Institutional Animal Care and Use Committee. PDX studies in mice were approved by the UVA Institutional Animal Care and Use Committee. Collection of human PDAC specimens was performed with approval of the Institutional Review Board at the University of Virginia in coordination with the Biorepository and Tissue Research Facility. All patients provided written informed consent for participation.

Data Availability

The data generated in this study are publicly available via the Gene Expression Omnibus dataset GSE252909. All other raw data are available upon request from the corresponding author. CPTAC PDAC Discovery Study clinical and histology data were obtained from the publication (4). Proteomics data were downloaded from the LinkedOmics data portal. TCGA PAAD RNA-seq gene expression data (data set ID: TCGA.PAAD.sampleMap/HiSeqV2; version: 2017-10-13) were downloaded from the UCSC Xena Browser. TCGA PAAD phenotype and survival data were also downloaded from UCSC Xena. Annotated, pre-processed PDAC scRNA-seq data (24) were provided by Dr. David Tuveson (Cold Spring Harbor Laboratory). Links to data repositories are provided in **Supp Table S1**. Code for the analysis of publicly available data is available at: https://github.com/lazzaralab/Brown-et-al_PDAC-hypoxia-EMT.

RESULTS

EMT correlates with hypoxia in human PDAC.

We first investigated a relationship between EMT and hypoxia in human PDAC using CPTAC mass spectrometry (4). Tumor clustering based on a pan-cancer EMT (pcEMT) signature (22) identified mesenchymal-high (M-high) and -low (M-low) groups **(Figure 1A)**. pcEMT was used because, unlike PDAC subtype signatures (10,11,13), it includes many typical EMT genes **(Supp Figure S1A,B)**, while also being useful for predicting disease-free survival **(Figure 1B)**. GSVA Hallmark Hypoxia enrichment scores were higher for M-high tumors **(Figure 1C)**. Importantly, only *COL5A1* is shared between Hallmark Hypoxia and pcEMT **(Supp Figure S1C)**, minimizing concerns about spurious correlations. High stromal tumor content (28) raises a potential concern for bulk analyses, but the mesenchymal-hypoxic relationship was preserved even when controlling for that issue **(Figure 1D)**. Repeating the analysis using a HIF target gene signature with no pcEMT overlap (23) also demonstrated that EMT preferentially occurs in hypoxic tumors **(Supp Figure S2A,B)**. We note that hypoxia was predictive of poor survival in the CPTAC PDAC cohort (4), and the mesenchymal pcEMT signature is enriched in hypoxic

CPTAC study tumors **(Supp Figure S2C)**. Despite little overlap between pcEMT and PDAC subtype signatures, M-high tumors largely align with Collisson quasi-mesenchymal, Moffitt basal-like, and Bailey squamous subtypes **(Figure 1A, Supp Figure S2D)**. Quasi-mesenchymal, basal-like, or squamous tumors are also enriched in Hallmark Hypoxia and HIF signatures **(Supp Figure S1D, Supp Figure S2E,F)**. Similar findings were obtained using TCGA RNA-sequencing **(Supp Figure S3A-G)**. Enrichment for hypoxia transcripts was predictive of lower disease-specific survival **(Supp Figure S3H)**, consistent with CPTAC PDAC study conclusions (4).

To study ductal cells specifically, we analyzed single-cell RNA-sequencing (scRNA-seq) from six human PDAC tumors (24) via two-dimensional UMAP and consensus clustering **(Figure 1E)**. Two groups emerged with markedly different mesenchymal gene expression **(Figure 1F)**. Hallmark Hypoxia **(Figure 1G)** and HIF target **(Supp Figure S4A)** signatures were significantly enriched in more mesenchymal cells. Ductal cells from a *Kras*$^{+/LSL\text{-}G12D}$*, Trp53*$^{+/LSL\text{-}R172H}$*, Pdx1-Cre* mouse model (24) exhibited similar relationships **(Supp Figure S4B-E)**. Thus, hypoxia and EMT are correlated in PDAC tumors.

Hypoxia promotes EMT in multiple PDAC model systems.

To explore the possibility of cell-autonomous hypoxia-mediated EMT, HPAF-II human PDAC cells were cultured for 120 hr in 21%, 7%, or 1% O_2. HPAF-II cells are baseline epithelial (29) and harbor three prevalent PDAC mutations (*Kras*^{G12D}, *TP53*, and *CDKN2A*) (30). Selected oxygen concentrations align with conditions in conventional cell culture (21%), normal pancreas (6.8%), and PDAC tumors (0.4%) (1,31). E-cadherin loss was robust by 120 hr in hypoxic culture, but hypoxia-inducible factor (HIF)-1α expression peaked at earlier times **(Supp Figure S5A,B)**. Early E-cadherin increases likely resulted from establishment of cell-cell contacts. At 1% O_2, ~25-30% of HPAF-II cells underwent EMT, based on increased vimentin expression and associated E-cadherin losses **(Figure 2A)**. Meaningful differences were not observed between

21% and 7% O_2, so subsequent experiments compared 21% and 1% O_2. For 1% O_2, E-cadherin and vimentin were inversely related **(Figure 2A)**, as expected, and vimentin was subsequently used as the primary EMT marker.

Other observations also suggested a *bona fide* EMT in hypoxia. In 1% O_2, GFP-expressing HPAF-II cell exhibited reduced cluster circularity and increased scatter **(Figure 2B)**, consistent with responses to growth factors (21). HPAF-II cells in 1% O_2 also exhibited increased expression of hypoxia markers *PGK1* and *SLC2A1* and mesenchymal transcripts *VIM*, *SNAI1*, and *TWIST1*, and decreased *CDH1* expression **(Figure 2C)**. Decreased *HIF1A* expression is consistent with prior reports (32).

PDX- and murine tumor-derived cells were also tested for cell-autonomous hypoxia-mediated EMT. For PDXs, we first confirmed by RNA-sequencing and tumor grading that mesenchymal genes were enriched in cells from poorly differentiated tumors **(Supp Figure S5C,D)**. Based on screening for epithelial traits by tissue microarray **(Supp Figure S5E-G)**, six PDX cell lines were evaluated. Cells from PDXs 366, 395, and 449 exhibited increased scatter or loss of epithelial morphology in 1% O_2 **(Supp Figure S5H)**. PDX 395 cells were studied further because they exhibited anticipated E-cadherin and vimentin changes. In pilot screening of six baseline epithelial KPCY cells, every line exhibited increased vimentin positivity in 1% O_2 **(Supp Figure S6A)**. 7160c2 was among those with an obvious morphology change and was used for further studies.

To investigate a hypoxia-EMT correlation *in vivo*, we confirmed the presence of hypoxic tumor regions in a mouse PDAC model using pimonidazole (Hypoxyprobe, HYP). Pilot studies showed abundant HYP tumor staining by six weeks **(Supp Figure S6B)**. Compared to normal mouse pancreas, a PDX tumor exhibited low CD31 endothelial and elevated HYP staining **(Figure 2D)**. CD31-positive capillary beds were non-overlapping with HYP-positive cells **(Figure 2E)**. To assess the EMT-hypoxia relationship, we used orthotopic PDX, KPCY autochthonous, and subcutaneous KPCY cell line models. Human COXIV or YFP was used to identify ductal

cells in PDX or implanted/autochthonous tumors, respectively **(Figure 2F-I, Supp Figure S6C-H)**. Because PDX 395 tumors are devoid of human fibroblasts (33), COXIV+ cells were identified as human ductal cells. In PDX tumors, COXIV+/HYP+ cells were primarily vimentin+ **(Figure 2F)**. Similarly, in KPCY and subcutaneous tumors, more YFP+/HYP+ cells were vimentin+ than were YFP+/HYP- **(Figure 2G,H, Supp Figure S6G)**. In KPCY subcutaneous tumors, YFP+/HYP+ cells exhibited reduced E-cadherin expression **(Figure 2I, Supp Figure S6H)**. Thus, hypoxic tumor regions are enriched for ductal cell EMT.

Hypoxia-driven EMT is more durable than growth factor-driven EMT.

To make a hypoxia comparison against growth factors, we combined TGFβ and HGF because both potently promote EMT. In HPAF-II cells, growth factors generated more than twice as many vimentin+ cells as hypoxia **(Figure 3A)**. E-cadherin expression was reduced by both growth factors and hypoxia **(Supp Figure S7A)**. By immunofluorescence microscopy, growth factors were again observed to be more potent in HPAF-II cells, but hypoxia and growth factors had comparable effects in PDX and KPCY cells **(Figure 3B)**.

To explore the time scales of mesenchymal persistence for different conditions, HPAF-II cells exposed to growth factors or 1% O_2 were replated in complete medium at 21% O_2. Interestingly, vimentin loss occurred more slowly for once-hypoxic cells than those treated with growth factors **(Figure 3C)**. Similar trends were observed in KPCY and PDX cell lines **(Supp Figure S7B,C)**. Replating KPCY and PDX cells after EMT induction caused a temporary spike in vimentin, potentially related to cytoskeletal adhesions. Despite this effect, more persistent vimentin expression was apparent for hypoxia.

Prolonged vimentin maintenance in once-hypoxic cells suggests a heritable trait. To test this, we quantified nuclei with a morphology indicative of mitosis 120 hr after relief of EMT-induction. The once-hypoxic population contained more actively dividing, vimentin-positive cells than those treated with growth factors, as determined by counting mitotic or Ki67-positive nuclei

(Figure 3D, Supp Figure S7D). Preferential vimentin persistence after hypoxia was still observable five weeks after treatment **(Supp Figure S7E)**.

To explore the implications of durable hypoxia-mediated EMT in tumors, HPAF-II cells were engineered with a HIF-regulated fate-mapping system that stably converts hypoxic cells from DsRed to GFP expression (26). Validation of the clonally selected transductant is described in **Supp Figure S7F**,**G**. Orthotopic tumors formed from the selected clone exhibited more vimentin+/HYP+ tumor cells than vimentin+/HYP- cells **(Supp Figure S7H)**, as expected. Surprisingly, there were equivalent numbers of GFP+/vimentin+ cells that were HYP+ or HYP- **(Figure 3E)**, potentially indicating that cells can maintain a hypoxia-driven mesenchymal state outside hypoxic domains. Five-color confocal imaging revealed similar vimentin positivity for DsRed+ and GFP+ cells **(Supp Figure S7H)**, suggesting that factors other than hypoxia (e.g., cytokines) drove EMT. To test the mesenchymal durability of GFP+ cells, explanted tumors were dissociated and flow-sorted into DsRed+, GFP+, and DsRed+/GFP+ populations, which were subsequently cultured in 21% O_2. Double-positive cells arise due to slow DsRed turnover, and very few collected cells were solely GFP+. 12 days after dissociation, more DsRed+/GFP+ cells were vimentin+ than were DsRed+ cells **(Figure 3F)**. Combined with Figure 3C results, this suggests that hypoxia-mediated EMT contributed substantially to vimentin expression in DsRed+/GFP+ cells.

MAPK and SFK signaling promote hypoxia-mediated EMT and are activated by impaired phosphatase expression.

To identify mechanisms that promote EMT in hypoxia, we first analyzed CPTAC proteomics (4). Reported overall kinase phosphorylation scores were extracted and Spearman rank correlation coefficients with Hallmark Hypoxia enrichment scores were calculated. The kinase list was then pared for an overrepresentation analysis of KEGG signaling pathways **(Supp Table S2)** by retaining kinases whose phosphorylation correlated positively and

significantly ($p < 0.05$) with Hallmark Hypoxia enrichment. The MAPK gene set had the largest number and fraction of phosphokinases present **(Figure 4A, Supp Figure S1E)**.

For scRNA-seq data (24), we developed a linear model of Hallmark Hypoxia enrichment dependence on KEGG signaling ontologies in ductal cells. We used LASSO regression for automatic variable selection, followed by ordinary least squares regression with variable selection by Akaike information criterion (AIC) minimization. Of the 30 KEGG signaling gene sets that were sufficiently overdispersed to obtain Pagoda2 scores, 19 were retained by LASSO, and 16 of these were retained by AIC. The final model was statistically significant and identified MAPK as the most predictive gene set **(Figure 4B)**. Identical analyses of mouse scRNA-seq (24) identified HIF-1 and MAPK signatures as most predictive of hypoxia enrichment **(Supp Figure S8A)**. We pursued MAPKs first based on this and returned to HIFs later.

We tested p38, JNK, and ERK1/2 inhibitors for antagonism of hypoxia-mediated EMT. Concentrations were chosen for their ability to impact EMT without causing cell death. MEK and JNK inhibitors suppressed vimentin and promoted E-cadherin expression in hypoxia **(Figure 4C, Supp Figure S8B,C)**. Surprisingly, p38 inhibition promoted vimentin expression, which could indicate a p38 role in EMT suppression (34). Combined inhibition of MEK and JNK had an additive effect, suggesting pathway cooperation. An additive effect was also seen for protein markers in PDX 395 cells **(Figure 4D)** and transcripts in HPAF-II cells **(Supp Figure S8D)**.

MAPKs play a prominent role in growth factor-driven EMT (21,35), and we compared MAPK induction for growth factors and hypoxia. For growth factors, c-Jun (a common name for the protein encoded by *JUN*), pc-Jun, and pERK abundances were increased by 24 hr and returned to baseline by 120 hr. In hypoxia, elevated c-Jun expression and ERK phosphorylation persisted at 120 hr, with concomitant E-cadherin reduction **(Figure 4E, Supp Figure S8E).** Because c-Jun expression changes were more robustly detected than phosphorylation changes at the latest time, expression was typically used as a JNK activity proxy. This choice is sensible because JNK activity promotes c-Jun expression (36) **(Supp Figure S8F)** and ERK1/2

knockdown does not alter c-Jun abundance **(Supp Figure S8G)**. siRNA-mediated knockdown of ERK1/2 and/or c-Jun **(Supp Fig S8G,H)** or stable shRNA-mediated knockdown of *ERK2* and *JUN* **(Supp Figure S8I-K)** also impeded hypoxia-mediated EMT.

To identify the MAPK signaling driver in hypoxia, two kinase arrays were used **(Supp Figure S9A,B)**. Both detected increased Src family kinase (SFK) phosphorylation. SFK inhibition antagonized nuclear c-Jun accumulation and ERK phosphorylation **(Figure 4F,G)**, consistent with known SFK roles, and antagonized hypoxia-driven EMT **(Figure 4H)**. Although hypoxia promotes TGFβ-dependent EMT in some settings (37), TGFβ receptor I (TGFβRI) inhibition had no effect on hypoxia-mediated EMT in HPAF-II cells **(Supp Figure S9C)**. Furthermore, TGFβ signaling was not nominated by analyses of patient data **(Figure 4A,B)**. A screen for cytokines (Luminex) did not identify any EMT-promoting candidates that were upregulated in hypoxic HPAF-II cells (Supp Figure S9D).

Lacking signaling-initiating cytokine leads, we hypothesized that hypoxia suppresses phosphatase expression and specifically considered protein phosphatase 2A (PP2A) due to its regulation of MAPK and SFK signaling (38). In patient scRNA-seq data (24), transcripts for subunits of PP2A, as well as PP2C and PP1A, were negatively correlated with the HIF gene signature **(Supp Figure S10)**. In HPAF-II cells, transcripts for multiple phosphatase subunits were decreased by hypoxia but not growth factors **(Figure 4I).** Furthermore, PP2A or PP2Cδ inhibition at 21% O_2 promoted vimentin expression **(Figure 4J)** and c-Jun and ERK nuclear accumulation **(Supp Figure S9E-G)**.

We next probed the relevance of MAPK signaling in mouse models. In KPCY and subcutaneous tumors, nuclear c-Jun was elevated in hypoxic YFP+ cells **(Figure 5A,B)**. In PDX tumors, nuclear c-Jun was also more abundant in hypoxic cells, and nuclear c-Jun was found preferentially in vimentin-positive cells **(Figure 5C)**. PDX tumors also exhibited elevated pERK in vimentin-positive cells **(Figure 5D)**. Interestingly, hypoxia-mediated EMT, while durable, was reversible via MEK and JNK inhibition in cell culture **(Figure 5E, Supp Figure S9H,I)**.

To investigate the ability of MAPK antagonism to abrogate EMT *in vivo*, MEK and JNK inhibitors were tested in orthotopic PDX 395 tumors. For both HYP+ and HYP- cells, MEK or JNK inhibition reduced vimentin positivity, but the effect was only significant with combined MEK and JNK inhibition **(Figure 5F, Supp Figure S9J,K)**. Thus, ERK and JNK cooperate to drive EMT in hypoxic tumor cells, and kinase inhibitors can interrupt and reverse this process even in poorly vascularized tissue.

HIFs play a supporting role in hypoxia-driven EMT.

To test the role of HIFs, we utilized RNA interference or gene knockouts. Transient knockdown of *HIF1A* (HIF-1α) and/or *EPAS1* (HIF-2α) in HPAF-II cells antagonized vimentin expression in hypoxia **(Figure 6A, Supp Figure S11A)**. However, there was no significant effect of HIF knockdown on *VIM*, *SNAI1*, or *CDH1* transcripts at 1% O_2 **(Figure 6B)**. Vimentin post-translational regulation (39) could account for the discrepancy, which was also observed with JNK inhibition **(Supp Figure S8D)**. Stable knockdown of both transcripts failed to reduce vimentin expression significantly **(Figure 6C, Supp Figure S11B)**. In tumor sections from a pancreas-specific, *Kras*-mutant *Hif1a*-knockout ($Kras^{G12D}Hif1a^{KO}$) mouse (3), we observed an insignificant change in vimentin-positivity in $Hif1a^{KO}$ versus *Hif1a*-replete tumors **(Supp Figure S11C)**. Because MAPKs regulate HIF expression (40), we tested the effects of MEK and JNK inhibitors on HIF abundance. Each inhibitor antagonized HIF-1α accumulation, and the combination of inhibitors was even more effective **(Figure 6D)**. *HIF1A* transcripts were unaffected **(Figure 6E)**, pointing to a post-translational stabilization by MAPKs. Collectively, these data suggest that HIFs play a supporting, but not indispensable, role in hypoxia-mediated EMT.

Hypoxia-driven EMT depends on histone methylation.

Due to the durable nature of hypoxia-driven EMT, we hypothesized that epigenetic modifications could be involved. TGFβ-mediated EMT requires histone H3 lysine 36 dimethylation (H3K36me2) and ensuing *Zeb1* and *Snai1* expression (16), and we thus focused on that mark. H3K36me2 abundance was significantly increased in HPAF-II cells treated with growth factors or 1% O_2 **(Figure 7A)**. Furthermore, H3K36me2 persisted longer in once-hypoxic cells than growth factor-treated cells **(Supp Figure S12A)**.

We next investigated effects on the lysine demethylase KDM2A and methyltransferase NSD2, which regulate H3K36me2 (16). Activities of the Jumonji C family lysine demethylases KDM5A and KDM6A are highly oxygen-dependent (18,19). We characterized the oxygen-dependent activity of KDM2A **(Supp Figure S12B-G)** and found a KDM2A-H3K36me2 interaction strength consistent with other demethylase/histone pairs (K_M = 108 ± 12 μM) and an O_2 K_M = 57 ± 17 μM **(Figure 7B,C, Supp Figure S12H)**. While this O_2 K_M is several-fold lower than those for KDM5A and KDM6A (18,19), it clearly falls between oxygen concentrations observed in normal pancreas (1.21-12.05%, or 11.9-118.6 μM) and PDAC tumors (0-0.69%, or 0-6.78 μM) (1,41). Thus, KDM2A activity should be substantially compromised in hypoxic PDAC tissue. Interestingly, *KDM2A* transcripts were slightly elevated by hypoxia **(Supp Figure S12I)**. While KDM2A expression is HIF-1α-dependent in some settings, this relationship was absent in HPAF-II cells **(Supp Figure S12I)**. KPCY cell lines (16) also displayed increased H3K36 dimethylation, accompanied by increased vimentin expression, in hypoxia **(Figure 7D, Supp Figure S12J)**.

We also found that NSD2 expression was augmented at 1% O_2 **(Figure 7E)**. Interestingly, *NSD2* transcripts were partially depleted by hypoxia, consistent with observations in patient scRNA-seq data **(Supp Figure S13A,B)**. Changes in *NSD2* abundance in hypoxia were insensitive to HIF-1α and HIF-2α knockdown or MEK and JNK inhibition **(Supp Figure S13C,D)**. Searching for possible post-translational mechanisms, we noted that dephosphorylation by PP2Cδ promotes NSD2 degradation (42) and recalled that *PPM1D*, which

encodes PP2Cδ, was depleted in hypoxia **(Figure 4I)**. Consistent with the implied mechanism, NSD2 expression was elevated by PP2Cδ inhibition, and to a lesser degree by PP2A inhibition **(Figure 7F)**. While NSD2 knockdown impeded H3K36 dimethylation in response to hypoxia or growth factors, it preferentially antagonized EMT in response to hypoxia **(Figure 7G, Supp Figure S13E)**. Hypoxia-mediated EMT and H3K36 dimethylation were also Nsd2- and Kdm2a-dependent in KPCY cell lines (16) **(Supp Figure S13F,G)**. Previously reported RNA-sequencing of these cell lines (16) reveals that PP2A and PP2C subunits, and dual-specificity phosphatases, were altered by *Kdm2a* or *Nsd2* knockout, providing a mechanistic link between histone methylation and MAPK activation. We further found that MEK and JNK inhibition antagonized H3K36 dimethylation and NSD2 expression in 1% O_2, but that NSD2 expression could be rescued by PP2Cδ co-inhibition **(Figure 7H)**. HIF-1α and/or HIF-2α knockdown also antagonized H3K36 dimethylation in 1% O_2 **(Supp Figure S13H).** Collectively, these results suggest that hypoxia reduces KDM2A activity, suppressing serine/threonine phosphatases and stabilizing NSD2.

DISCUSSION

Our results show that hypoxia and EMT are so typically related in PDAC that statistically significant relationships can be determined from three types of patient data and four mouse models. In the mechanism we propose **(Figure 8)**, hypoxia reduces KDM2A activity, resulting in H3K36 dimethylation and decreased protein phosphatase expression. Loss of phosphatases, such as PP2A, promotes SFK and MAPK signaling, which cooperates with reduced PP2Cδ activity to stabilize NSD2, creating a reinforcing, positive feedback that leads to durable EMT. ERK and JNK also stabilize HIF-1α, which plays a supporting role. Collectively, ERK, JNK, and H3K36me2 promote expression of c-Jun, HIF-1α and other EMT transcription factors.

Uncertainty remains about the rate-limiting step for epithelial reversion after hypoxic cells are returned to a normoxic environment. Previously hypoxic cells revert to an epithelial state

quickly after kinase inhibitors are applied. Thus, one possibility is that hypoxic mesenchymal cells become stuck in a pseudo-equilibrium that can be reversed by severe intervention. That pseudo-equilibrium state may arise preferentially for hypoxia because of the extreme loss of KDM2A activity that occurs. Interestingly, EMT exhibits path-dependent bistable or tristable states (43), but this effect has not previously been reported for hypoxia. MAPK (44) and HIF-1α (45) signaling also exhibit bistability.

Previous work identified MAPK pathways as targets for PDAC combination therapy. MEK/ERK inhibitors have been combined with PD-L1 antibodies (46) and PI3K inhibitors (47), and low-dose "vertical inhibition" of RAF and ERK promotes epithelial characteristics in KRAS-mutant PDAC (48). ERK1/2 inhibitor monotherapy for PDAC is ineffective due to an autophagic response, but combined ERK and autophagy inhibition suppresses tumor growth (49). JNK signaling is activated in PDAC by 5-fluorouracil plus leucovorin (5-FU+LEU) or FOLFOX (5-FU+LEU plus oxaliplatin), and JNK inhibition reduces FOLFOX chemoresistance (50). Our findings motivate pursuing combinations of MAPK inhibitors for antagonism of hypoxia-mediated EMT, which may increase chemoresponse.

Epigenetic changes other than H3K36me2, including histone 3 lysine 4 acetylation (H3K4Ac), H3K4me2, and H3K27me3, regulate EMT genes (51,52). We focused on H3K36me2 given its known role in PDAC EMT (16). Enzymes that modify epigenetic marks are also being tested as drugs targets, with early-phase trials in solid tumors (53). Inhibitors have been identified against methyltransferases (54), the methyltransferase enhancer EZH2 (53), and histone deacetylases (HDAC) (55). HDAC inhibition alone is ineffective in PDAC (56), but combined HDAC and MEK inhibitors hold promise (57). NSD2 inhibitors target the methyl-transferring SET domain are also in development (58).

While the hypoxic NSD2 accumulation we observed was post-translationally regulated, others have reported HIF-1α-dependent *NSD2* accumulation in melanoma cells (59). Thus, different mechanisms may regulate NSD2 abundance in hypoxia. Several core HIF-binding sites

(5'-RCGTG-3') (60) exist in the *NSD2* promoter. However, other transcription factors cooperate with HIFs in a tissue- and gene-specific manner (61), which may explain why HIFs do not universally regulate *NSD2* (60). Hypoxia can also regulate NSD2 through downregulation of PP2Cδ, which dephosphorylates and destabilizes NSD2 (42), and through MAPK activity. The latter effect may occur via NSD2 PEST domains, which can slow protein turnover when phosphorylated (62). The online tool ePESTfind reports that NSD2 has two regions (531 – 546 and 615 – 656) with high PEST scores (>5). The online iGPS algorithm (63) with a lenient threshold predicts that JNK and ERK phosphorylate NSD2 threonine 544 and serines 631 and 639.

Hypoxia also promotes metabolic changes that contribute to aggressive disease (64), and metabolic reprogramming can be accompanied by EMT (65). Hypoxia-mediated expression of the mesenchymal protein N-cadherin is glucose- and glutamine-dependent, indicating that glycolytic and glutaminolytic activity influence hypoxia-mediated EMT (66). Further, MEK and JNK are involved in the Warburg effect by interacting with key metabolic regulators in glycolysis (67), and some epigenetic modifiers respond to altered intracellular energy levels (68). Potential metabolic dependencies in the mechanism we elucidated should be explored.

Finally, the durable nature of hypoxia-mediated EMT could make this mechanism especially likely to contribute to metastatic dissemination. At the same time, our finding that hypoxia-driven EMT can persist for weeks may challenge the typical view that a mesenchymal-epithelial transition is required for metastatic outgrowth. Additional work is needed to investigate these issues.

ACKNOWLEDGEMENTS

The authors thank Danielle Gilkes (Johns Hopkins) for the hypoxia fate-mapping plasmids and technical discussions, David Tuveson (Cold Springs Harbor Laboratory) for sharing annotated scRNAseq data, John Tobias (University of Pennsylvania) and Shayn Peirce-Cottler (UVA) for technical discussions, Yi Zhang (Harvard) for creating the *KDM2A* plasmid, Jing-Yi Chen (I-Shou University) for sharing the *KDM2A* plasmid, Kevin Janes (UVA) for the eGFP plasmid, Carl June (University of Pennsylvania) and Paolo Provenzano (University of Minnesota) for cell lines, Robert Norgard (University of Pennsylvania) for assistance providing KPCY tumor sections, Mark Yeager (UVA) for the pFastBac1 plasmid, and CPTAC PDAC Discovery Study senior authors for technical discussions. Figure 8 was created with BioRender.com.

FUNDING

This work was supported by NCI U01 CA243007 (MJL), NSF 1716537 (MJL), NSF 1700687 (MJL), NSF Graduate Research Fellowship 1842490 (BAB), UVA Cancer Training Program T32CA009109, UVA Biomedical Data Sciences Training Program T32LM012416, and UVA Cancer Center Support Grant NCI P30CA044579.

REFERENCES

1. Koong AC, Mehta VK, Le QT, Fisher GA, Terris DJ, Brown JM*, et al.* Pancreatic tumors show high levels of hypoxia. Int J Radiat Oncol Biol Phys **2000**;48:919-22
2. Katsuta E, Qi Q, Peng X, Hochwald SN, Yan L, Takabe K. Pancreatic adenocarcinomas with mature blood vessels have better overall survival. Sci Rep **2019**;9:1310
3. Lee KE, Spata M, Bayne LJ, Buza EL, Durham AC, Allman D*, et al.* Hif1a Deletion Reveals Pro-Neoplastic Function of B Cells in Pancreatic Neoplasia. Cancer Discov **2016**;6:256-69
4. Cao L, Huang C, Cui Zhou D, Hu Y, Lih TM, Savage SR*, et al.* Proteogenomic characterization of pancreatic ductal adenocarcinoma. Cell **2021**;184:5031-52 e26
5. Chang Q, Jurisica I, Do T, Hedley DW. Hypoxia predicts aggressive growth and spontaneous metastasis formation from orthotopically grown primary xenografts of human pancreatic cancer. Cancer Res **2011**;71:3110-20
6. Chen S, Chen JZ, Zhang JQ, Chen HX, Yan ML, Huang L*, et al.* Hypoxia induces TWIST-activated epithelial-mesenchymal transition and proliferation of pancreatic cancer cells in vitro and in nude mice. Cancer Lett **2016**;383:73-84
7. Zhang Q, Lou Y, Zhang J, Fu Q, Wei T, Sun X*, et al.* Hypoxia-inducible factor-2alpha promotes tumor progression and has crosstalk with Wnt/beta-catenin signaling in pancreatic cancer. Mol Cancer **2017**;16:119
8. Rhim AD, Mirek ET, Aiello NM, Maitra A, Bailey JM, McAllister F*, et al.* EMT and dissemination precede pancreatic tumor formation. Cell **2012**;148:349-61
9. Aiello NM, Maddipati R, Norgard RJ, Balli D, Li J, Yuan S*, et al.* EMT Subtype Influences Epithelial Plasticity and Mode of Cell Migration. Dev Cell **2018**;45:681-95 e4
10. Bailey P, Chang DK, Nones K, Johns AL, Patch AM, Gingras MC*, et al.* Genomic analyses identify molecular subtypes of pancreatic cancer. Nature **2016**;531:47-52
11. Collisson EA, Sadanandam A, Olson P, Gibb WJ, Truitt M, Gu S*, et al.* Subtypes of pancreatic ductal adenocarcinoma and their differing responses to therapy. Nat Med **2011**;17:500-3
12. Dijk F, Veenstra VL, Soer EC, Dings MPG, Zhao L, Halfwerk JB*, et al.* Unsupervised class discovery in pancreatic ductal adenocarcinoma reveals cell-intrinsic mesenchymal features and high concordance between existing classification systems. Sci Rep **2020**;10:337
13. Moffitt RA, Marayati R, Flate EL, Volmar KE, Loeza SG, Hoadley KA*, et al.* Virtual microdissection identifies distinct tumor- and stroma-specific subtypes of pancreatic ductal adenocarcinoma. Nat Genet **2015**;47:1168-78
14. Lu W, Kang Y. Epithelial-Mesenchymal Plasticity in Cancer Progression and Metastasis. Dev Cell **2019**;49:361-74
15. Bashir M, Damineni S, Mukherjee G, Kondaiah P. Activin-A signaling promotes epithelial-mesenchymal transition, invasion, and metastatic growth of breast cancer. NPJ Breast Cancer **2015**;1:15007
16. Yuan S, Natesan R, Sanchez-Rivera FJ, Li J, Bhanu NV, Yamazoe T*, et al.* Global Regulation of the Histone Mark H3K36me2 Underlies Epithelial Plasticity and Metastatic Progression. Cancer Discov **2020**;10:854-71
17. Losman JA, Koivunen P, Kaelin WG, Jr. 2-Oxoglutarate-dependent dioxygenases in cancer. Nat Rev Cancer **2020**;20:710-26
18. Chakraborty AA, Laukka T, Myllykoski M, Ringel AE, Booker MA, Tolstorukov MY*, et al.* Histone demethylase KDM6A directly senses oxygen to control chromatin and cell fate. Science **2019**;363:1217-22
19. Batie M, Frost J, Frost M, Wilson JW, Schofield P, Rocha S. Hypoxia induces rapid changes to histone methylation and reprograms chromatin. Science **2019**;363:1222-6

20. Chen B, Li L, Li M, Wang X. HIF1A expression correlates with increased tumor immune and stromal signatures and aggressive phenotypes in human cancers. Cell Oncol (Dordr) **2020**;43:877-88
21. Buonato JM, Lan IS, Lazzara MJ. EGF augments TGFbeta-induced epithelial-mesenchymal transition by promoting SHP2 binding to GAB1. J Cell Sci **2015**;128:3898-909
22. Mak MP, Tong P, Diao L, Cardnell RJ, Gibbons DL, William WN*, et al.* A Patient-Derived, Pan-Cancer EMT Signature Identifies Global Molecular Alterations and Immune Target Enrichment Following Epithelial-to-Mesenchymal Transition. Clin Cancer Res **2016**;22:609-20
23. Li B, Qiu B, Lee DS, Walton ZE, Ochocki JD, Mathew LK*, et al.* Fructose-1,6-bisphosphatase opposes renal carcinoma progression. Nature **2014**;513:251-5
24. Elyada E, Bolisetty M, Laise P, Flynn WF, Courtois ET, Burkhart RA*, et al.* Cross-Species Single-Cell Analysis of Pancreatic Ductal Adenocarcinoma Reveals Antigen-Presenting Cancer-Associated Fibroblasts. Cancer Discov **2019**;9:1102-23
25. Walters DM, Stokes JB, Adair SJ, Stelow EB, Borgman CA, Lowrey BT*, et al.* Clinical, molecular and genetic validation of a murine orthotopic xenograft model of pancreatic adenocarcinoma using fresh human specimens. PLoS One **2013**;8:e77065
26. Godet I, Shin YJ, Ju JA, Ye IC, Wang G, Gilkes DM. Fate-mapping post-hypoxic tumor cells reveals a ROS-resistant phenotype that promotes metastasis. Nat Commun **2019**;10:4862
27. Stirling DR, Swain-Bowden MJ, Lucas AM, Carpenter AE, Cimini BA, Goodman A. CellProfiler 4: improvements in speed, utility and usability. BMC Bioinformatics **2021**;22:433
28. Dhani NC, Serra S, Pintilie M, Schwock J, Xu J, Gallinger S*, et al.* Analysis of the intra- and intertumoral heterogeneity of hypoxia in pancreatic cancer patients receiving the nitroimidazole tracer pimonidazole. Br J Cancer **2015**;113:864-71
29. Rajasekaran SA, Gopal J, Espineda C, Ryazantsev S, Schneeberger EE, Rajasekaran AK. HPAF-II, a cell culture model to study pancreatic epithelial cell structure and function. Pancreas **2004**;29:e77-83
30. Moore PS, Sipos B, Orlandini S, Sorio C, Real FX, Lemoine NR*, et al.* Genetic profile of 22 pancreatic carcinoma cell lines. Analysis of K-ras, p53, p16 and DPC4/Smad4. Virchows Arch **2001**;439:798-802
31. McKeown SR. Defining normoxia, physoxia and hypoxia in tumours-implications for treatment response. Br J Radiol **2014**;87:20130676
32. Lin Q, Cong X, Yun Z. Differential hypoxic regulation of hypoxia-inducible factors 1alpha and 2alpha. Mol Cancer Res **2011**;9:757-65
33. Stokes JB, Adair SJ, Slack-Davis JK, Walters DM, Tilghman RW, Hershey ED*, et al.* Inhibition of focal adhesion kinase by PF-562,271 inhibits the growth and metastasis of pancreatic cancer concomitant with altering the tumor microenvironment. Mol Cancer Ther **2011**;10:2135-45
34. Strippoli R, Benedicto I, Foronda M, Perez-Lozano ML, Sanchez-Perales S, Lopez-Cabrera M*, et al.* p38 maintains E-cadherin expression by modulating TAK1-NF-kappa B during epithelial-to-mesenchymal transition. J Cell Sci **2010**;123:4321-31
35. Buonato JM, Lazzara MJ. ERK1/2 blockade prevents epithelial-mesenchymal transition in lung cancer cells and promotes their sensitivity to EGFR inhibition. Cancer Res **2014**;74:309-19
36. Kayahara M, Wang X, Tournier C. Selective regulation of c-jun gene expression by mitogen-activated protein kinases via the 12-o-tetradecanoylphorbol-13-acetate-responsive element and myocyte enhancer factor 2 binding sites. Mol Cell Biol **2005**;25:3784-92

37. Matsuoka J, Yashiro M, Doi Y, Fuyuhiro Y, Kato Y, Shinto O*, et al.* Hypoxia stimulates the EMT of gastric cancer cells through autocrine TGFbeta signaling. PLoS One **2013**;8:e62310
38. Hu X, Wu X, Xu J, Zhou J, Han X, Guo J. Src kinase up-regulates the ERK cascade through inactivation of protein phosphatase 2A following cerebral ischemia. BMC Neurosci **2009**;10:74
39. Snider NT, Omary MB. Post-translational modifications of intermediate filament proteins: mechanisms and functions. Nat Rev Mol Cell Biol **2014**;15:163-77
40. Furcht CM, Buonato JM, Skuli N, Mathew LK, Munoz Rojas AR, Simon MC*, et al.* Multivariate signaling regulation by SHP2 differentially controls proliferation and therapeutic response in glioma cells. J Cell Sci **2014**;127:3555-67
41. Ast T, Mootha VK. Oxygen and mammalian cell culture: are we repeating the experiment of Dr. Ox? Nat Metab **2019**;1:858-60
42. Lv N, Jin S, Liang Z, Wu X, Kang Y, Su L*, et al.* PP2Cdelta Controls the Differentiation and Function of Dendritic Cells Through Regulating the NSD2/mTORC2/ACLY Pathway. Front Immunol **2021**;12:751409
43. Jia D, Jolly MK, Tripathi SC, Den Hollander P, Huang B, Lu M*, et al.* Distinguishing mechanisms underlying EMT tristability. Cancer Converg **2017**;1:2
44. Legewie S, Schoeberl B, Bluthgen N, Herzel H. Competing docking interactions can bring about bistability in the MAPK cascade. Biophys J **2007**;93:2279-88
45. Fabian Z, Taylor CT, Nguyen LK. Understanding complexity in the HIF signaling pathway using systems biology and mathematical modeling. J Mol Med (Berl) **2016**;94:377-90
46. Henry KE, Mack KN, Nagle VL, Cornejo M, Michel AO, Fox IL*, et al.* ERK Inhibition Improves Anti-PD-L1 Immune Checkpoint Blockade in Preclinical Pancreatic Ductal Adenocarcinoma. Mol Cancer Ther **2021**;20:2026-34
47. Alagesan B, Contino G, Guimaraes AR, Corcoran RB, Deshpande V, Wojtkiewicz GR*, et al.* Combined MEK and PI3K inhibition in a mouse model of pancreatic cancer. Clin Cancer Res **2015**;21:396-404
48. Ozkan-Dagliyan I, Diehl JN, George SD, Schaefer A, Papke B, Klotz-Noack K*, et al.* Low-Dose Vertical Inhibition of the RAF-MEK-ERK Cascade Causes Apoptotic Death of KRAS Mutant Cancers. Cell Rep **2020**;31:107764
49. Bryant KL, Stalnecker CA, Zeitouni D, Klomp JE, Peng S, Tikunov AP*, et al.* Combination of ERK and autophagy inhibition as a treatment approach for pancreatic cancer. Nat Med **2019**;25:628-40
50. Lipner MB, Peng XL, Jin C, Xu Y, Gao Y, East MP*, et al.* Irreversible JNK1-JUN inhibition by JNK-IN-8 sensitizes pancreatic cancer to 5-FU/FOLFOX chemotherapy. JCI Insight **2020**;5
51. Lin YT, Wu KJ. Epigenetic regulation of epithelial-mesenchymal transition: focusing on hypoxia and TGF-beta signaling. J Biomed Sci **2020**;27:39
52. Wu MZ, Tsai YP, Yang MH, Huang CH, Chang SY, Chang CC*, et al.* Interplay between HDAC3 and WDR5 is essential for hypoxia-induced epithelial-mesenchymal transition. Mol Cell **2011**;43:811-22
53. Chen Y, Ren B, Yang J, Wang H, Yang G, Xu R*, et al.* The role of histone methylation in the development of digestive cancers: a potential direction for cancer management. Signal Transduct Target Ther **2020**;5:143
54. Dong B, Qiu Z, Wu Y. Tackle Epithelial-Mesenchymal Transition With Epigenetic Drugs in Cancer. Front Pharmacol **2020**;11:596239
55. Dovzhanskiy DI, Arnold SM, Hackert T, Oehme I, Witt O, Felix K*, et al.* Experimental in vivo and in vitro treatment with a new histone deacetylase inhibitor belinostat inhibits the growth of pancreatic cancer. BMC Cancer **2012**;12:226

56. Nguyen AH, Elliott IA, Wu N, Matsumura C, Vogelauer M, Attar N*, et al.* Histone deacetylase inhibitors provoke a tumor supportive phenotype in pancreatic cancer associated fibroblasts. Oncotarget **2017**;8:19074-88
57. Chao MW, Chang LH, Tu HJ, Chang CD, Lai MJ, Chen YY*, et al.* Combination treatment strategy for pancreatic cancer involving the novel HDAC inhibitor MPT0E028 with a MEK inhibitor beyond K-Ras status. Clin Epigenetics **2019**;11:85
58. Wang S, Yang H, Su M, Lian F, Cong Z, Wei R*, et al.* 5-Aminonaphthalene derivatives as selective nonnucleoside nuclear receptor binding SET domain-protein 2 (NSD2) inhibitors for the treatment of multiple myeloma. Eur J Med Chem **2021**;222:113592
59. Xu Y, Guo J, Liu J, Xie Y, Li X, Jiang H*, et al.* Hypoxia-induced CREB cooperates MMSET to modify chromatin and promote DKK1 expression in multiple myeloma. Oncogene **2021**;40:1231-41
60. Schodel J, Oikonomopoulos S, Ragoussis J, Pugh CW, Ratcliffe PJ, Mole DR. High-resolution genome-wide mapping of HIF-binding sites by ChIP-seq. Blood **2011**;117:e207-17
61. Wenger RH, Stiehl DP, Camenisch G. Integration of oxygen signaling at the consensus HRE. Sci STKE **2005**;2005:re12
62. Day EK, Campbell A, Pandolf A, Rogerson T, Zhong Q, Xiao A*, et al.* ERK-dependent suicide gene therapy for selective targeting of RTK/RAS-driven cancers. Mol Ther **2021**;29:1585-601
63. Song C, Ye M, Liu Z, Cheng H, Jiang X, Han G*, et al.* Systematic analysis of protein phosphorylation networks from phosphoproteomic data. Mol Cell Proteomics **2012**;11:1070-83
64. Vasseur S, Tomasini R, Tournaire R, Iovanna JL. Hypoxia induced tumor metabolic switch contributes to pancreatic cancer aggressiveness. Cancers (Basel) **2010**;2:2138-52
65. Jia D, Park JH, Kaur H, Jung KH, Yang S, Tripathi S*, et al.* Towards decoding the coupled decision-making of metabolism and epithelial-to-mesenchymal transition in cancer. Br J Cancer **2021**;124:1902-11
66. Guillaumond F, Leca J, Olivares O, Lavaut MN, Vidal N, Berthezene P*, et al.* Strengthened glycolysis under hypoxia supports tumor symbiosis and hexosamine biosynthesis in pancreatic adenocarcinoma. Proc Natl Acad Sci U S A **2013**;110:3919-24
67. Papa S, Choy PM, Bubici C. The ERK and JNK pathways in the regulation of metabolic reprogramming. Oncogene **2019**;38:2223-40
68. Teperino R, Schoonjans K, Auwerx J. Histone methyl transferases and demethylases; can they link metabolism and transcription? Cell Metab **2010**;12:321-7

FIGURE LEGENDS

Figure 1. EMT and hypoxia marker enrichment are correlated in human PDAC tumors and ductal cells. (A) CPTAC PDAC tumor samples were clustered using non-negative matrix factorization (NMF) of protein data for the pcEMT signature. Heatmap entries indicate z-scored expression. Left vertical side bar (green, purple) indicates assigned NMF cluster. The next three vertical side bars indicate Collisson, Moffit, and Bailey classifications (4). Horizontal side bar (red, blue) indicates phenotype associated with each protein (22). **(B)** Kaplan-Meier analysis for CPTAC PDAC patient survival, stratifying based on pcEMT with log-rank test. **(C)** Hallmark Hypoxia protein enrichment was calculated using GSVA and compared between M-high and -low tumors, with Mann-Whitney U test. **(D)** Partial rank correlation coefficients (PRCCs) of indicated variables were calculated with respect to mesenchymal pcEMT (pcEMT-M) enrichment. Hallmark Hypoxia enrichment from calculations in (C). Tissue content estimates were from CPTAC data. Error bars denote PRCC 95% confidence intervals. **(E)** Consensus clustering of human ductal cell scRNA-seq data (24) was performed on a 2D UMAP based on pcEMT-M features, resulting in groupings with shared epithelial features but differentially enriched for mesenchymal features (E+/M- and E+/M+). **(F)** Heatmap showing ductal cell pcEMT gene expression (normalized UMIs), annotated by clusters from (E). **(G)** mRNA enrichment of Hallmark Hypoxia signature (Pagoda2 scores) was computed and compared between E+/M+ and E+/M- ductal cells, Mann-Whitney U test.

Figure 2. Hypoxia drives a *bona fide* EMT in PDAC. (A) HPAF-II cells were cultured at 21%, 7%, or 1% O_2 for 120 hr, and immunofluorescence microscopy was performed as indicated, n = 3. One-way ANOVA with Tukey's multiple comparison test (vimentin). Mixed-effects analysis with Tukey's multiple comparison test (E-cadherin). Linear regression for E-cadherin and vimentin described in *Methods*. **(B)** GFP-expressing HPAF-II cells were cultured in 21% or 1% O_2 for 96 hr. Fluorescence microscopy was performed, and cluster shape factors were calculated. Data represented as mean ± s.e.m. $p < 0.0001$ for slopes comparison, see *Methods*. **(C)** HPAF-II cells were cultured for 120 hr in 21% or 1% O_2, and qRT-PCR was performed for indicated markers, with *CASC3* used for normalization. n = 3, with t test per transcript. **(D)** H&E and immunohistochemistry for Hypoxyprobe (HYP) and CD31 was performed for murine normal pancreas and PDX tumors. Representative image shown, n = 3. **(E)** Sections of normal mouse pancreas or PDX 395 tumors were stained as indicated. Image analysis was performed for PDX 395 tumors and quantified for the percent CD31+ cells that were HYP+/-. n = 3, t test. **(F)** PDX 395 tumor sections were stained to quantify COXIV+/vimentin+ cells that were HYP+/-. n = 4, t test. Dotted line separates HYP+/- regions. **(G)** KPCY tumor sections were stained as indicated, and image analysis was performed to quantify YFP+/vimentin+ cells that were HYP+/-. Data represented as fold-change due to variability across mice for the spontaneous model. n = 4, t test. **(H)** Subcutaneous PD7591 cell tumors were stained as indicated, with quantification of YFP+/vimentin+ cells that were HYP+/-. n = 6, t test. **(I)** PD7591 cell subcutaneous tumor sections were stained as indicated, with quantification for YFP+/HYP+ cells that were $Ecad^{high/low}$. Arrow denotes an HYP+/$Ecad^{low}$ cell. n = 4, with t test. * $p < 0.05$, ** $p < 0.01$, *** $p < 0.001$, **** $p < 0.0001$

Figure 3. Hypoxia-driven EMT occurs heterogeneously and is more durable than growth factor-driven EMT. (A) HPAF-II cells were cultured in 21% O_2 ± 10 ng/mL TGFβ and 50 ng/mL HGF or cultured in 1% O_2 for 120 hr. Vimentin flow cytometry was performed. Representative histograms for single replicates are shown, with data for n = 3 in the bar plot. One-way ANOVA with Tukey's pairwise comparisons against the 21% O_2 control. **(B)** PDAC cells from three backgrounds were cultured as in (A). Immunofluorescence microscopy was performed as indicated. n = 3, two-way ANOVA with Tukey's multiple comparisons test. **(C)** HPAF-II cells

were cultured as in (A), re-plated on coverslips, and cultured in 21% O_2 without growth factors for ≤ 120 hr. At indicated times, immunofluorescence microscopy was performed as indicated. *n* = 3, data represented as mean ± s.e.m. $p < 0.0001$ for nonlinear regression comparing slopes. **(D)** 120 hr after treatment withdrawal from 10 ng/mL TGFβ + 50 ng/mL HGF or 1% O_2 culture. HPAF-II cells were stained to quantify dividing, vimentin+ cells (examples encircled). *n* = 3, with t test. **(E)** Orthotopic HPAF-II hypoxia fate-mapping tumor sections were stained as indicated. Image analysis quantified fraction of GFP+ (once-hypoxic) cells that were vimentin+ and Hypoxyprobe-negative (HYP-) or positive (HYP+). *n* = 6, with t test. **(F)** Explanted tumors described in (E) were disaggregated and flow-sorted based on DsRed and GFP. Indicated populations were cultured in 21% O_2 for 12 days, then stained with indicated antibodies. *n* = 4, with t test. * $p < 0.05$, ** $p < 0.01$, **** $p < 0.0001$

Figure 4. Hypoxia promotes EMT through MAPK signaling initiated by suppressed phosphatase expression. (A) Overrepresentation analysis for indicated KEGG pathways based on kinases described in the text. Analysis based on CPTAC PDAC Discovery Study data (4). Kinase count and ratio indicate the number and fraction in each gene set with significant, positive correlations with Hallmark Hypoxia enrichment. **(B)** Coefficients are shown for regularized linear regression of Hallmark Hypoxia Pagoda2 score based on KEGG signaling pathway Pagoda2 scores for scRNA-seq data (24). Error bars denote 95% confidence intervals. **(C)** HPAF-II cells were cultured for 120 hr in 21% or 1% O_2 with 1 μM CI-1040 (MEKi), 10 μM SP600125 (JNKi), 10 μM SB203580 (p38i), or DMSO. *n* = 3, two-way ANOVA with Sidak's multiple comparisons test. **(D)** PDX 395 cells were cultured in 1% O_2 with 1 μM CI-1040 (MEKi), 10 μM SP600125 (JNKi), a combination, or DMSO for 120 hr. Cells were stained as indicated, and immunofluorescence microscopy and image analysis were performed. *n* = 3, one-way ANOVA with Dunnett's multiple comparison test. **(E)** HPAF-II cells were cultured in 21% O_2 ± 10 ng/mL TGFβ + 50 ng/mL HGF, or in 1% O_2, and lysed 24 and 120 hr after treatment. Immunoblotting was performed as indicated. *n* = 3, one-way ANOVA with Tukey's multiple comparisons test. **(F)** HPAF-II cells were cultured for 120 hr in 21 or 1% O_2 with 10 μM PP2 (Src family kinase inhibitor, SFKi) or DMSO, and immunofluorescence microscopy was performed for nuclear c-Jun. *n* = 3, mixed-effects analysis with Tukey's multiple comparisons test. **(G)** HPAF-II cells were treated as in (F), and lysates were analyzed by immunoblotting as indicated. *n* = 3**,** two-way ANOVA with Sidak's multiple comparison test. **(H)** HPAF-II cells were cultured in 21% O_2 ± 10 ng/mL TGFβ and 50 ng/mL HGF or in 1% O_2 for 120 hr. Cells were pre-treated with 10 μM PP2 or DMSO 24 hr prior to hypoxia or growth factor treatment. *n* = 3, two-way ANOVA with Sidak's multiple comparison test. **(I)** qRT-PCR was performed for PP1A, PP2A, and PP2C subunit transcripts for HPAF-II cells treated as in (D) for 120 hr, with *CASC3* used for normalization. *n* = 3, one-way ANOVA with Tukey's multiple comparisons test. **(J)** HPAF-II cells were cultured for 120 hr in 21% O_2 with 5 μM LB100 (PP2Ai), 1.5 μM sanguinarine chloride (PP2Cδi), or DMSO. *n* = 3, one-way ANOVA with Tukey's multiple comparisons test. * $p < 0.05$, ** $p < 0.01$, *** $p < 0.001$, **** $p < 0.0001$

Figure 5. Hypoxic PDAC tissue is enriched for MAPK markers, and MAPK inhibition prevents hypoxic cell EMT. (A) KPCY tumor sections were stained as indicated, and YFP+/c-Jun+ cells that were Hypoxyprobe (HYP) +/- were quantified and reported as fold-changes from HYP- to HYP+. *n* = 3, with t test. Dotted line separates HYP+/- regions. **(B)** 7160c2 subcutaneous tumor sections were stained as indicated, and image analysis was performed as in (A). *n* = 4, with t test. **(C)** PDX 395 orthotopic tumor sections were stained as indicated, and c-Jun+ cells that were HYP+/- or vimentin+/- were quantified. c-Jun+ data reported as fold-change in percent c-Jun+ cells that were HYP+/-. *n* = 3, with t test. **(D)** PDX 395 tumor sections were stained as indicated, and the percent of vimentin+/- cells that were pERK+ was quantified. *n* = 3, with t test. **(E)** HPAF-II cells were cultured in 21% O_2 ± 10 ng/mL TGFβ + 50 ng/mL HGF

or in 1% O_2 for 120 hr. Cells were re-plated for 120 hr at 21% O_2 without exogenous growth factors and with 1 μM CI-1040 (MEKi) and 10 μM SP600125 (JNKi) or DMSO. At times indicated, cells were stained for vimentin. Immunofluorescence microscopy was performed to quantify percentage of vimentin+ cells. *n* = 3, two-way ANOVA with Tukey's multiple comparisons test. **(F)** Mice bearing orthotopic PDX 395 tumors were treated for nine days with selumetinib (MEKi), SP600125 (JNKi), selumetinib+SP600125, or vehicle. Tumor sections were stained for COXIV, HYP, and vimentin, and image analysis was performed. *n* = 5 - 6, two-way ANOVA with Tukey's multiple comparisons test. * $p < 0.05$, ** $p < 0.01$, *** $p < 0.001$, **** $p < 0.0001$

Figure 6. HIFs play a supporting role in hypoxia-mediated EMT. (A,B) HPAF-II cells were transfected with HIF-1α or HIF-2α siRNA, both siRNAs, or control siRNA. 24 hr later, cells were switched to 1% O_2 or maintained in 21% O_2 for 120 hr. **(A)** Immunofluorescence microscopy was performed, with quantification for vimentin+ cells. *n* = 3, two-way ANOVA with Tukey's multiple comparisons test. **(B)** qRT-PCR was performed for indicated transcripts, with *CASC3* used for normalization. *n* = 3, two-way ANOVA with Tukey's multiple comparisons test. **(C)** Immunofluorescence microscopy was performed on HPAF-II cells stably expressing HIF-1α and HIF-2α or control shRNAs. Cells were cultured in 21% or 1% O_2 for 120 hr prior to fixing and staining as indicated. *n* = 3, two-way ANOVA with Tukey's multiple comparisons test. **(D)** HPAF-II cells were pre-treated with 1 μM CI-1040 (MEKi), 10 μM SP600125 (JNKi), a combination, or DMSO for 24 hr, then cultured in 21 or 1% O_2 for 4 hr. *n* = 3, two-way ANOVA with Tukey's multiple comparisons test. **(E)** *HIF1A* qRT-PCR was performed for HPAF-II cells cultured for 120 hr in 21% or 1% O_2 with 1 μM CI-1040 (MEKi),10 μM SP600125 (JNKi), a combination, or DMSO. *CASC3* used as normalization control. *n* = 3, two-way ANOVA with Tukey's multiple comparisons test, comparisons against controls. * $p < 0.05$, ** $p < 0.01$, *** $p < 0.001$, **** $p < 0.0001$

Figure 7. Hypoxia reduces KDM2A activity and stabilizes NSD2 to promote histone methylation-dependent EMT. (A) HPAF-II cells were cultured in 21% O_2 ± 10 ng/mL TGFβ + 50 ng/mL HGF or in 1% O_2 for 120 hr, and H3K36 dimethylation (H3K36me2) was measured by immunofluorescence microscopy. *n* = 3, mixed-effects analysis with Tukey's multiple comparisons test. **(B-C)** Michaelis-Menten saturation curves were created with Lineweaver-Burk plots for KDM2A binding kinetics for **(B)** H3K36me2 and **(C)** oxygen, with velocity (*V*) reported as disintegration parts per minute (dpm). Data shown for a representative run, with solid lines corresponding to model fits. **(D)** KPCY-derived cell lines 3077c4, 6419c5, and 6694c2 were cultured in 21% or 1% O_2 for 120 hr. Cells were then fixed and stained as indicated, and immunofluorescence microscopy was performed. *n* = 3, mixed-effects analysis for H3K36me2 per cell line. **(E)** Immunofluorescence microscopy was performed for NSD2 expression in HPAF-II cells treated as in (A). *n* = 3, mixed-effects analysis with Tukey's multiple comparisons test. **(F)** HPAF-II cells were cultured for 120 hr in 21% O_2 with 5 μM LB100 (PP2Ai), 1.5 μM sanguinarine chloride (PP2Cδi), or DMSO. Immunofluorescence microscopy was performed for NSD2. *n* = 3, mixed-effects analysis with Tukey's multiple comparisons. **(G)** HPAF-II cells were transfected with control or NSD2 siRNA. 24 hr later, cells were treated as in (A) for 120 hr. Immunofluorescence microscopy was performed as indicated. *n* = 3, two-way ANOVA for vimentin positivity with Sidak's multiple comparisons test and mixed-effects analysis for H3K36me2 with Tukey's multiple comparisons test. **(H)** HPAF-II cells were cultured in 1% O_2 with 1 μM CI-1040 (MEKi), 10 μM SP600125 (JNKi), and 1.5 μM sanguinarine chloride (PP2Cδi), or DMSO for 120 hr. *n* = 3, mixed-effects analysis with Tukey's multiple comparisons test. * $p < 0.05$, ** $p < 0.01$, *** $p < 0.001$

Figure 8. Hypoxia promotes EMT through an integrated histone methylation and MAPK mechanism. Hypoxia suppresses KDM2A activity resulting in dimethylation of H3K36, which in turn suppresses expression of protein phosphatase subunits. Decreased protein phosphatase expression promotes SFK and MAPK signaling to stabilize NSD2, HIF-1α, and nuclear c-Jun expression. Elevated NSD2 expression further promotes H3K36 dimethylation, reinforcing the integrated kinase signaling/histone methylation regulatory loop. Collectively, this promotes expression of EMT-regulating genes.

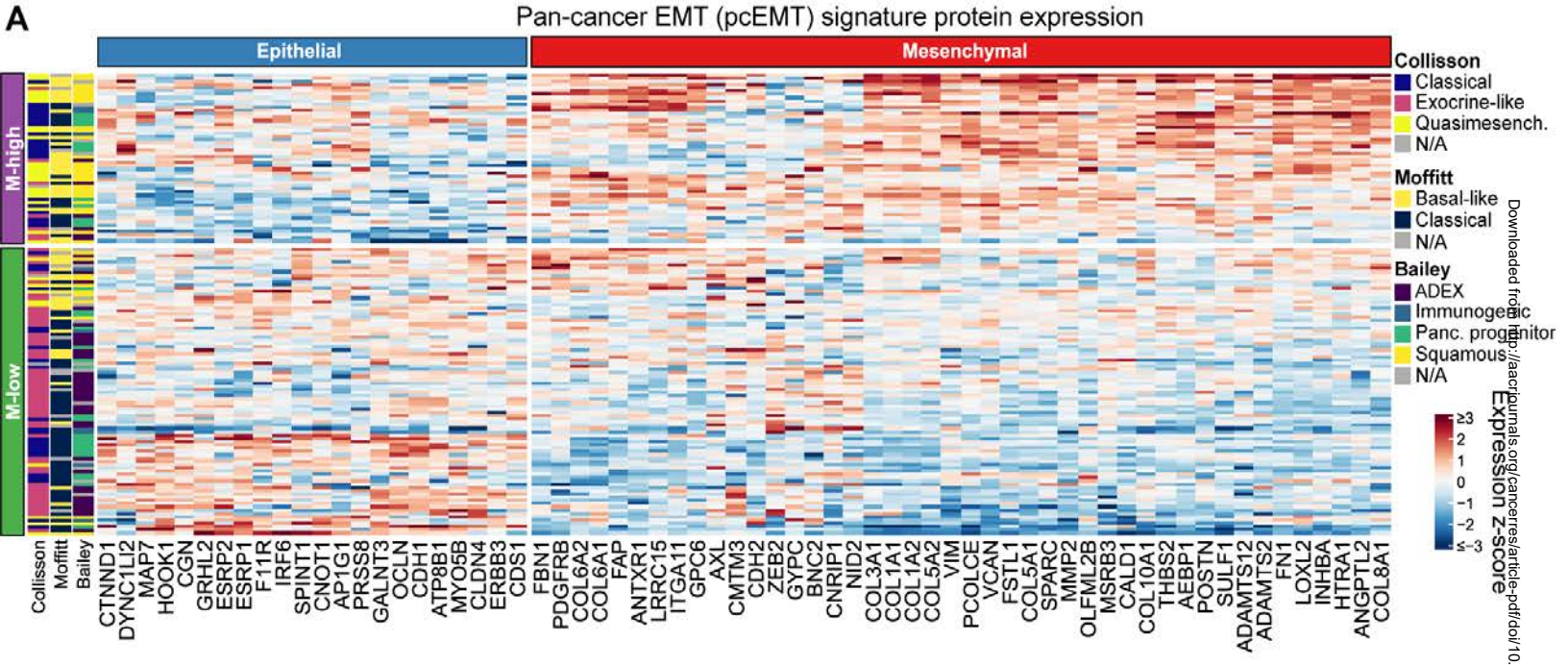

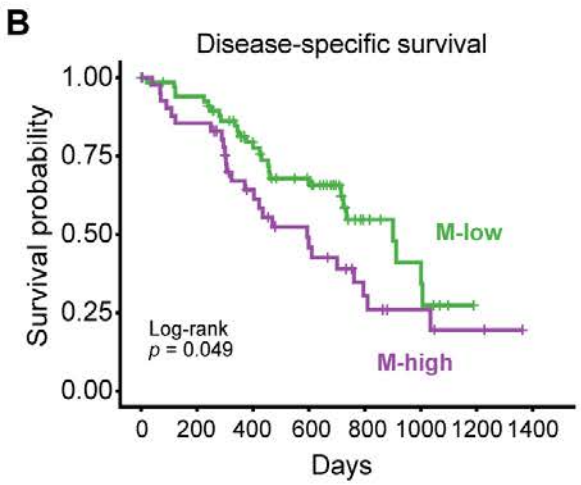

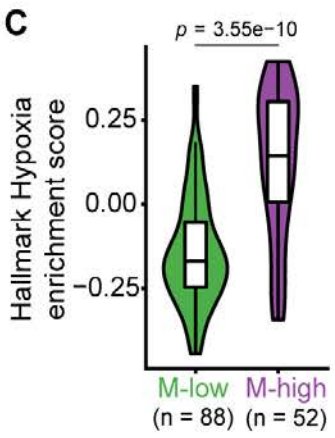

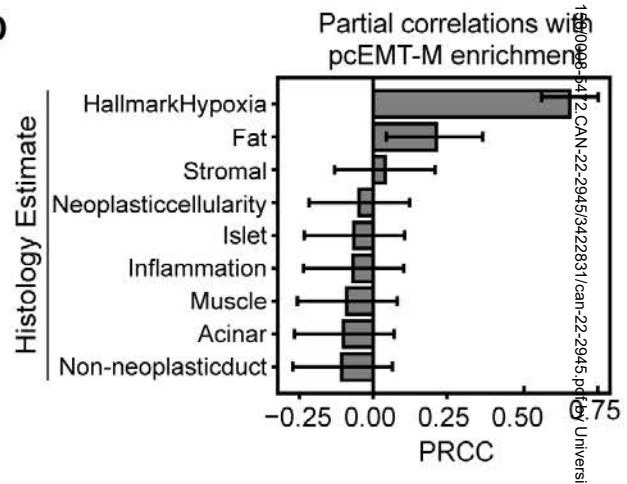

Single-Cell RNA-Sequencing: Human Ductal Cells

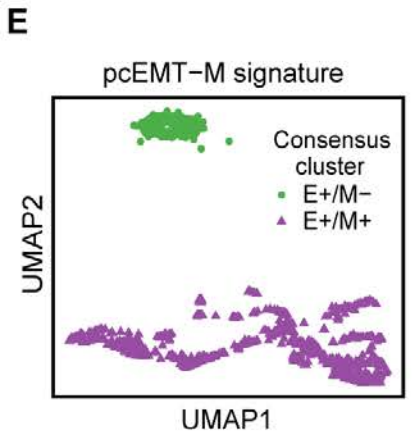

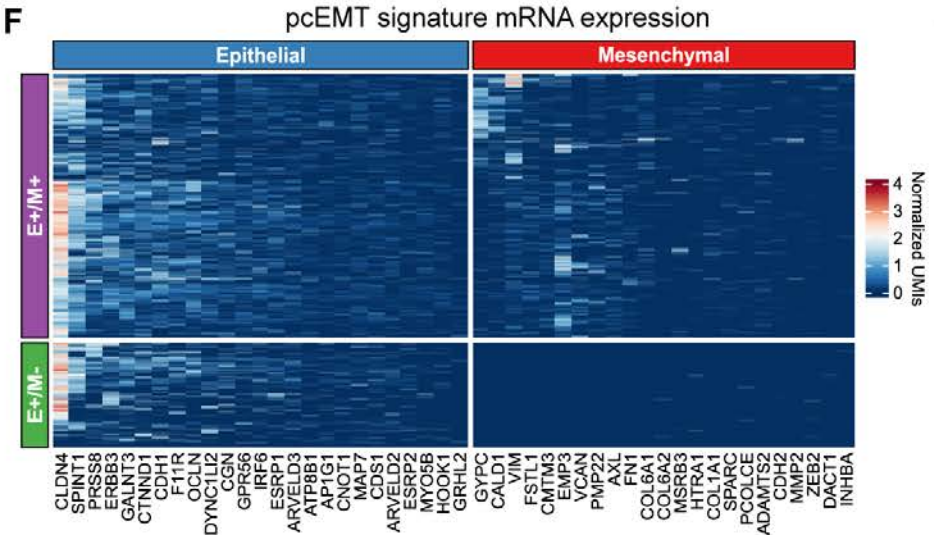

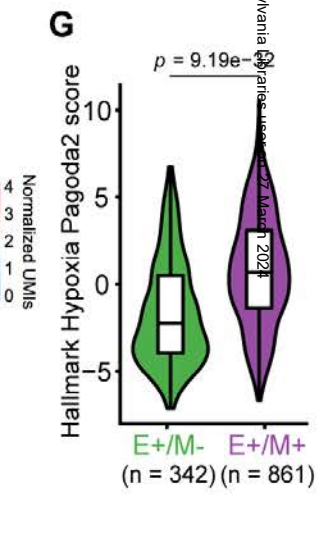

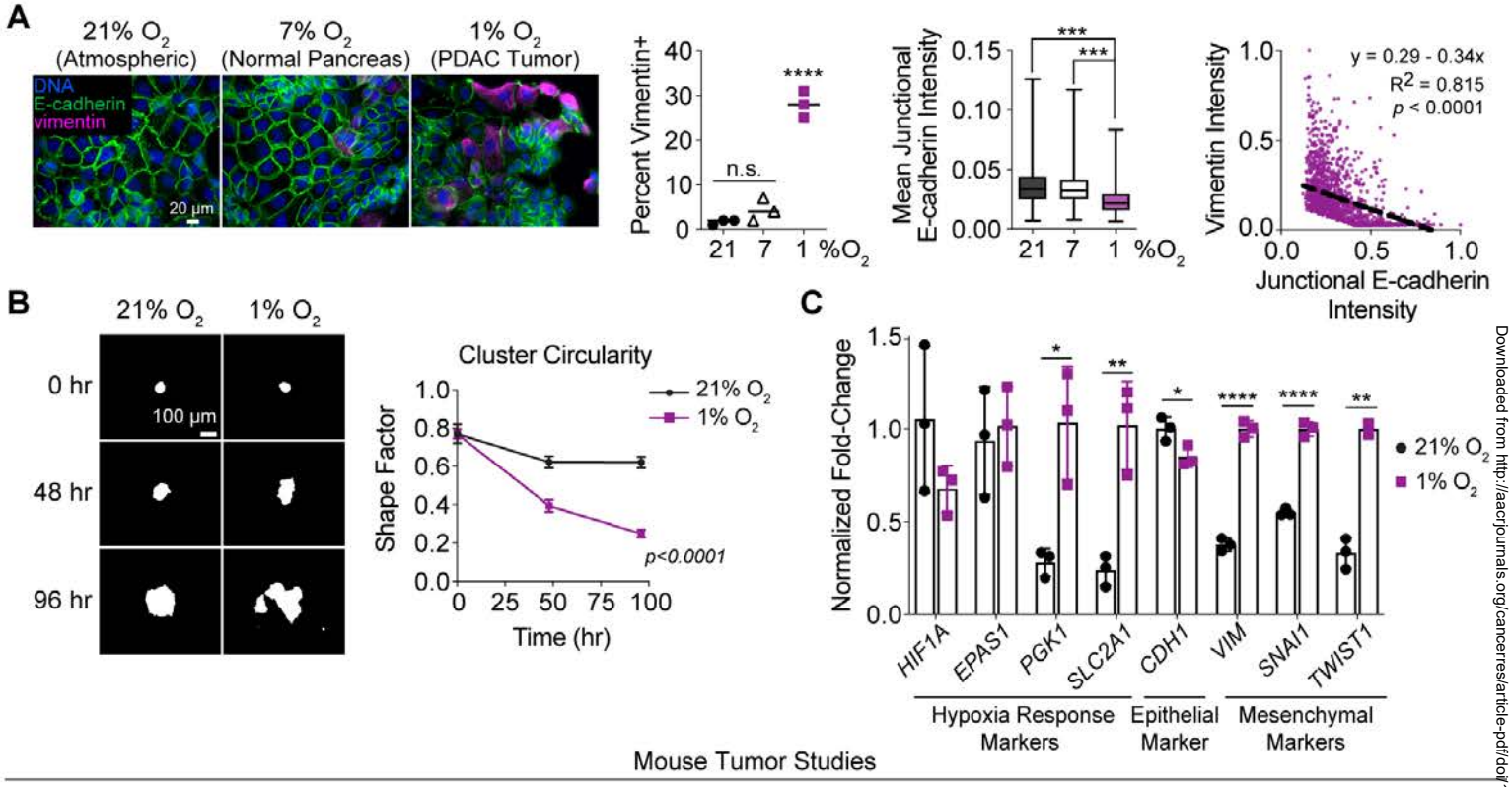

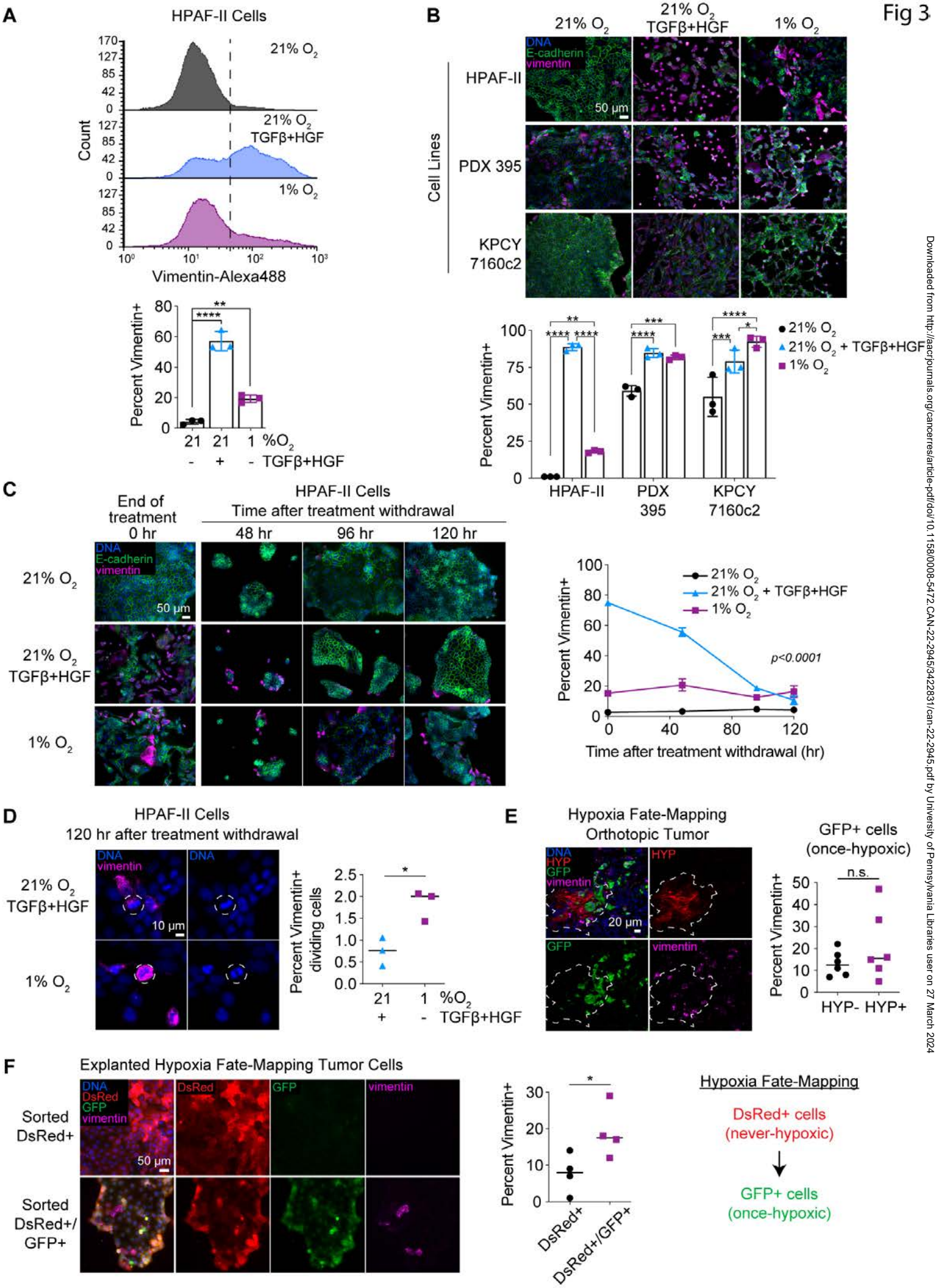

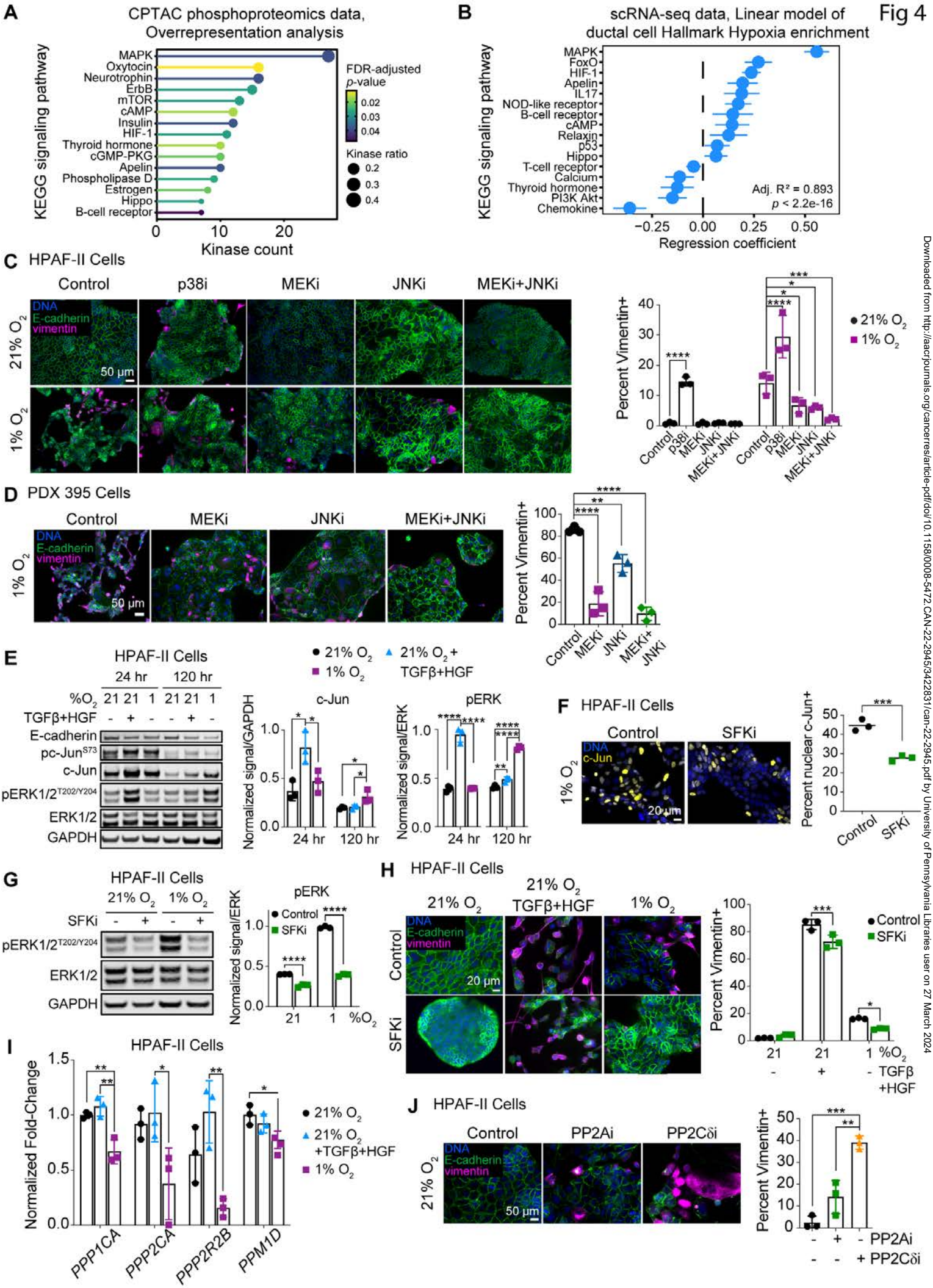

Fig 5